CHALMERS
UNIVERSITY OF TECHNOLOGY

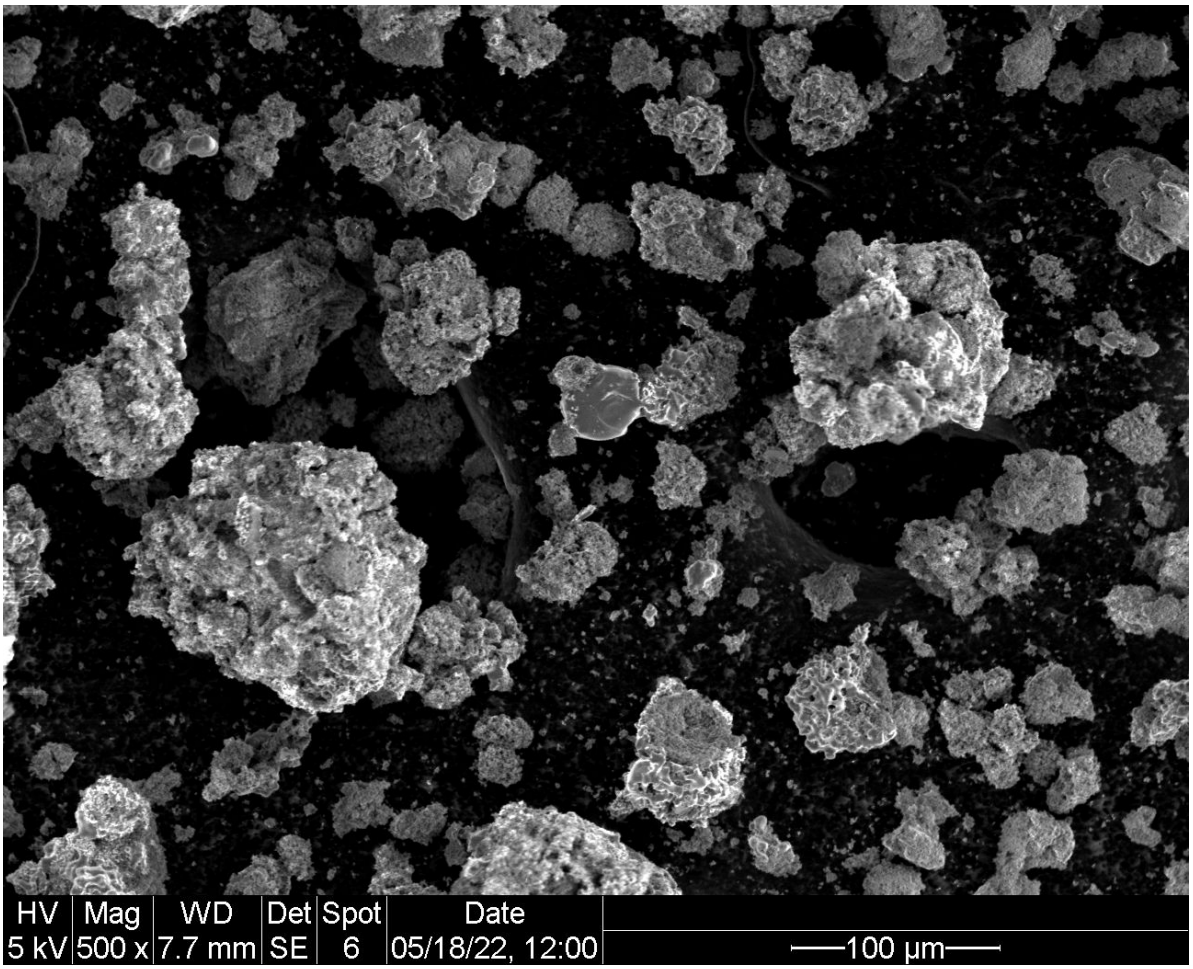

Synthesis and characterisation of TiAl/Al_2O_3 for high-temperature applications

Master's thesis in Materials Engineering

Shravan Ranjith

DEPARTMENT OF INDUSTRIAL AND MATERIALS SCIENCE
CHALMERS UNIVERSITY OF TECHNOLOGY
Gothenburg, Sweden 2022
www.chalmers.se

Master's thesis 2022

Synthesis and characterisation of $TiAl/Al_2O_3$ for high-temperature applications

SHRAVAN RANJITH

CHALMERS
UNIVERSITY OF TECHNOLOGY

Department of Industrial and Materials Science
Division of Materials and Manufacture
Chalmers University of Technology
Gothenburg, Sweden 2022

Synthesis and characterisation of $TiAl/Al_2O_3$ for high-temperature applications
SHRAVAN RANJITH

Supervisor: Dr. Laura Cordova Gonzalez, Department of Industrial and Materials Science
Co-Supervisor: Dr. Gorgees Adam
Examiner: Prof. Eduard Hryha, Department of Industrial and Materials Science

Master's Thesis 2022
Department of Industrial and Materials Science
Chalmers University of Technology
SE-412 96 Gothenburg

Cover image: Scanning electron microscopy image of $TiAl/Al_2O_3$ powder, showing coarsened particles as a result of synthesis in argon atmosphere.
Typeset in LaTeX
Printed by Chalmers Reproservice
Gothenburg, Sweden 2022

Synthesis and characterisation of $TiAl/Al_2O_3$ for high-temperature applications
SHRAVAN RANJITH
Department of Industrial and Materials Science
Chalmers University of Technology

Abstract

There is an increasing demand for new materials to improve engine efficiency and keep up with the regulations in the aerospace sector. The titanium aluminide (TiAl) has been a material of interest mainly because of the properties such as low density, high stiffness, and high creep resistance. In addition, aluminium oxide (Al_2O_3) as reinforcement particles allows to improve corrosion resistance and mechanical properties. Metal matrix composites (MMCs) can attain superior mechanical and thermal properties because of the reinforced matrix. These materials could be processed by surface coating on low value parts as well, extending its pool of applications to marine, chemical and other applications.

In this master thesis, the synthesis of $TiAl/Al_2O_3$, titanium metal matrix composite material from titanium dioxide (TiO_2) and aluminium (Al) will be investigated. Ball milling and synthesis at high temperature have been employed to attain the phase transformation to $TiAl/Al_2O_3$. During synthesis, the effect and influence of argon (Ar) and hydrogen (H_2) atmospheres on the final composite was studied. Oxygen analysis and thermogravimetric analyses were used to follow material synthesis in this study. X-ray diffraction peaks confirmed the phase transformation from TiO_2 and Al to $TiAl/Al_2O_3$. The final particle morphology was characterised using scanning electron microscopy (SEM) and light optical microscopy (LOM).

Keywords: Titanium aluminide, Aluminium oxide, Ball milling, Metal powder, High temperature synthesis, Processing atmosphere.

Acknowledgements

I would like to thank Prof.Eduard Hryha for mentoring me during the project and Dr.Laura Cordova Gonzalez for the support throughout the duration of the thesis project. I would also like to thank Dr.Gorgees Adam for sharing his expertise with the material and his guidance.

I sincerely thank the Department of Industrial and Materials Science (IMS), Division of Materials and Manufacture for providing the workplace and equipments used during the project and also Höganäs AB for the x-ray diffraction analysis and oxygen analysis done at their facility. I would also like to thank Centre for Additive Manufacture (CAM2) for funding this thesis project.

I am deeply indebted to Dr.Yiming Yao, Dr.Antonio Mulone, Sri Bala Aditya Malladi, Xiaolong Li, Anok Babu Nagaram, Erika Steyn and Bharat Mehta for supporting me with training and sharing their practical experiences that helped me structure the thesis.

My interest towards materials engineering was intrigued while working in utilisation of Al dross headed by Dr.Parvati Ramaswamy, who as a mentor guided and nurtured me to a better student. I would like to thank her for the knowledge and passion that she has passed down to me.

I would like to take this opportunity to thank Vishnu Anilkumar for sharing his experience and practical knowledge that was helpful during the laboratory work. Also, I would like to thank my friends Arda Baytaroglu, Changjie Huang, Renald George Swamy, Ezgi Ceren Boz Noyan, Fardan Ahmed and Claudia de Andrade Schwerz for making my time at Chalmers University and master thesis work at the department a memorable one.

Finally, I would like to thank my family for supporting my passion for materials engineering and all the professors for sharing their knowledge and experiences.

Shravan Ranjith, Gothenburg, June 2022

List of Acronyms

Below is the list of acronyms that have been used throughout this thesis listed in alphabetical order:

Al	Aluminium
Al_2O_3	Aluminium oxide
BCC	Body centered cubic
BSE	Back scattered electrons
DSC	Differential scanning calorimetry
EDS	Energy dispersive spectroscopy
HCP	Hexagonal closed pack
IMC	Intermetallic matrix composite
LOM	Light optical microscopy
LPS	Liquid phase sintering
RPM	Rotations per minute
SE	Secondary electron
SEM	Scanning electron microscope
STA	Simultaneous thermal analysis
TG	Thermogravimetry
TGA	Thermogravimetric Analysis
Ti	Titanium
TiAl	Titanium aluminide
TiH_2	Titanium hydride
TiO_2	Titanium oxide
TMMC	Titanium metal matrix composite
XRD	X-ray diffraction

Contents

List of Figures

List of Tables

1

Motivation

Intermetallics present both high temperature strength and high temperature creep resistance [Nakamura(1995)] making them an ideal class of materials for aerospace applications. Titanium aluminide (TiAl) has properties such as high specific strength, low density and good creep properties. A suitable reinforcement, Al_2O_3 with properties such as high melting point and hardness, can improve further capabilities as intermetallic composite (IMC). Aerospace industry as one of the highly regulated sectors, constantly demands new materials to enhance its efficiency. This can be possible by utilising the potential of such intermetallic composites, for example, to fulfil the demand to improve engine efficiency. Since the existing materials for these applications present limitations, new materials capable of increasing engine efficiency are needed. For example, materials consolidated by thermal spray to form layers of compounds resistant to the high operating temperatures of engines.

The intermetallic forms of Ti are the focus of this study because they enhance mechanical and thermal properties of materials [Lütjering and Williams(2007)]. TiAl is an intermetallic with considerable properties, in addition to the previously mentioned properties, such as high melting point, high elastic modulus, high specific strength, low density and good oxidation resistance [Binh(2021)].

Aluminium oxide (Al_2O_3) is a chemical compound commonly called alumina. Al_2O_3 is widely used in engineering and biomedical applications because of its properties [Nissan et al.(2008)Nissan, Choi, and Cordingley]. It can attain high density with pressureless means, such as sintering in the air. It also possesses mechanical properties such as wear resistance, high strength, high stiffness and also thermal properties such as high temperature oxidation resistance, high corrosion resistance and chemical inertness [Ruys(2018)]. To make use of these properties into industrial applications, one of the major consolidation routes to consider is processing the powder for high temperature application.

Therefore, there is an increasing interest to investigate the potential of TiAl/Al_2O_3 because, Al_2O_3 particles are compatible to Ti in order to synthesise TiAl and also since it improved the hardness of TiAl, makes Al_2O_3 a suitable reinforcement for TiAl [Binh(2021), Taotao(2008)]. This can possibly allow full utilisation of the properties of TiAl along with Al_2O_3 for high temperature applications.

1.1 Aim

This Master's thesis aims to study the potential of synthesising $TiAl/Al_2O_3$ from TiO_2 and Al to pave the way for the future industrial production and upscaling of lightweight intermetallic composites based on aluminium and titanium. In order to achieve it, three objectives were formulated:

- Evaluate and test the feasibility to synthesise $TiAl/Al_2O_3$ composite following a reaction equation.
- Mixing and synthesis of $TiAl/Al_2O_3$ using ball milling followed by a thermal treatment.
- Analysis of the phase transformation into $TiAl/Al_2O_3$ from TiO_2 and Al during synthesis using different processing atmospheres.

2
Theory

This chapter covers theoretical concepts on raw materials, ball milling, reaction mechanisms and the effect of the selected atmospheres during the synthesis.

2.1 Titanium

Titanium has been a popular material with density [4.5 g/cm^3] between that of aluminium and steel. It also possesses strength which is a characteristic of alloy steels [Froes(2015)]. Other than Ti and its alloys as an aerospace material, it has found its way to medical applications and sports equipments because of its bio-compatibility and lightweight respectively.

In fact, recent research has focused on the development of titanium metal matrix composites (TMMC) because of its properties, such as high strength, excellent corrosion, and heat resistance [Kondoh(2015)]. The conventional ingot metallurgy to fabricate TMMC with reinforcement is not suitable because of the high reactivity of Ti with oxygen. Hence, powder metallurgy is the most adopted processing route for the fabrication of TMMC parts [Kondoh(2015)].

2.1.1 Crystal structure

Pure titanium undergoes an allotropic transformation at 882 ° C from body-centred cubic (BCC) crystal structure β phase at high temperature and hexagonal closed pack (HCP)-α phase at low temperatures.
This temperature at which this transformation occurs is called β transus temperature, which depends on the purity of the element. At room temperature, the lattice parameters, a and c are 0.295 nm and 0.468 nm respectively for α titanium resulting in a c/a ratio of 1.587 which is close to the c/a ideal ratio of 1.633 for HCP crystal structure [Lütjering and Williams(2007)].

2.1.2 Titanium dioxide

Titanium dioxide (TiO_2) can be crystallized in three different forms: rutile, anatase, and brookite. Out of the three crystal structures, rutile and anatase are the most popular ones, being anatase more reactive than rutile [Pan and et.al.(1997)].
The basic building block structure of TiO_2 is represented in a pictorial form in [Lütjering and Williams(2007)] representing a Ti atom (white) surrounded by six

oxygen atoms (red) in an octahedral configuration. Since TiO phases in the TiO phase diagram have an extensive number of stable phases, TiO_2 can be reduced easily [Diebold(2003)].

2.1.3 Intermetallic compounds of titanium

Intermetallics form as a result of the combination of metals. This type of material possesses superior properties such as high melting temperatures which is partly contributed by the strong bonding between unlike atoms which are in general a combination of metallic, covalent, and ionic bonds. They hold the property of long-range order which contributes to low diffusivity. Therefore, alloys that have the property of dislocation climb are dependent on the diffusivity rate. Since the intermetallics have low diffusivity, the material will have a low creep rate which results in a higher creep resistance [Froes(2015)].

Titanium forms two intermetallic compounds with aluminium, mainly TiAl and Ti_3Al. TiAl has been the main intermetallic for application since Ti_3Al could not find the commercial gain compared to TiAl. In addition to that, TiAl has been an intermetallic of choice mainly because of its high-temperature creep behaviour that occurs as a result of dislocation movement difficulties under stress [Froes(2015)].

2.1.4 Titanium aluminide

TiAl usually consists of two major phases. They are α_2-Ti_3Al with hexagonal D019 structure and γ-TiAl phase with tetragonal L10 structure, which provides the ductility to TiAl [Chen and Li(2019)].

TiAl-based alloys have been a material of interest specifically in aerospace and automotive sectors because of their properties such as low density, high stiffness, high strength, high oxidation and creep resistance. They are of importance for the aerospace industry as they possess properties, that allow them to improve the thrust-to-weight ratio of aircraft engines, engine efficiency and fuel efficiency. Despite being an attractive material, since intermetallics possess long-range order, it results in low ductility at room temperature and fracture toughness. Because of this, the material becomes difficult to machine. Therefore, processing by powder metallurgy is preferred as it can reduce defects such as centerline porosity, uneven densities and microstructures, chemical inhomogeneity, grain refinement, finer and homogeneous structure, and also reduce the cost of the final resulting product [Chen and Li(2019), Liu and Liu(2015), Ivanova(2021)].

2.2 Aluminium

Aluminium (Al) is the third most abundantly present element in the Earth's crust. The potential of Al alloys have been understood widely before being used in industry [Lumley(2010)]. An oxide form of Al, Al_2O_3 has also gained importance in the industry due to its potential properties.

2.2.1 Aluminium oxide

Al_2O_3 is a material which is highly inert and also possesses corrosion resistance in an in-vivo environment. It exists naturally as corundum. It is extracted for commercial purposes from ores of Bauxite mainly by Bayer's process. It is a material of high hardness making it suitable to be used as abrasive, its high melting point makes it a suitable refractory material. Al_2O_3 exists in many crystal phases due to the heat treatment conditions such as $\alpha, \beta, \gamma, \eta, \theta, \rho$ and X. Among these phases, α alumina is the most thermodynamically stable phase [Ruys(2018)].

2.3 Metal matrix composites

Metal matrix composites (MMC) consist of a metal or an alloy as the matrix which is reinforced by particles or fibres of long or short sizes [Chawla(2012)].
There are four types of MMC:

- Particles reinforced MMC
- Continuous fibre MMC
- Short fibre MMC
- Monofilament reinforced metals

Out of the four types of MMCs, particles reinforced MMC are of interest for this project. Particles reinforced MMC consists of particles that are reinforced onto a metal or alloy matrix [Evans(2003)]. One of the prominent choices for the metal matrix is titanium alloys. Due to the combination with reinforcement particles, it improves the properties of titanium alloys, making them very suitable for high-temperature applications.

2.4 Ball milling

Ball milling uses a high-energy ball mill to process powders of pure metals, intermetallics, or pre-alloyed powders which possess a uniform composition [Suryanarayana(2001)].

When processing with ball milling, the morphology of the powder particles deform based on ductile-brittle mechanisms. On the one hand, the ductile particles become flattened and result in cold welding with other particles. On the other hand, brittle powder particles suffer fragmentation into smaller particles. In the case of a combination of brittle and ductile powder particles, the ductile powder particles deform and results in cold welding. This leads to the attachment of brittle particles to the ductile particles and to the formation of composite materials [Suryanarayana(2001)].

Following a list of the different types of mills:

- Spex shaker mills
- Planetary ball mills
- Attritor mills

From these four types of mills, planetary ball mills will be discussed in the further section, since planetary ball mill was used in this study.

2.4.1 Planetary ball mill

The name is derived from its working principle, which comprises of vials or crucibles that follow a moving pattern like planets around the supporting disk. The vial/crucible in the milling machine will rotate because of the operating mechanism, along with the particles to be milled and balls. The supporting disk in the milling machine will move in opposite direction to the rotation of the vial. This movement results in grinding because of the balls rotating along the inner circumference of the vial, as presented in section 4.3.2, Figure 4.5 of mechanical alloying and milling book [Suryanarayana(2001)]. Because of friction between the balls and the vial, powders in between will get ground. Along with this, the grinding balls collide with each other and produce an intense impact on the powder particles that are trapped in between. The impact energy because of the collision of balls mainly depends on the rotational speed of the vial. It is important to note that, if the speed of the vial is too low, the impact energy of the balls reduces and then the required milling process is limited or even non-existing [Suryanarayana(2001)].

2.5 Sintering

Sintering is the heat treatment with or without pressure assistance to bond powder particles into, mainly a solid structure by mass transportation mechanism in the atomic scale. While sintering, the spherical particles in contact will form a neck between them as a result of the rising temperature and diffusion. The atomic motion from the surface of the particles to the neck reduces the total surface energy while neck growth occurs. This gradually leads to a full material densification. [German(2010)].

2.5.1 Sintering in powder mixtures

In the case of sintering mixed powders, it is possible to achieve the dispersion of one phase in the matrix to improve the properties of the resulting composite.
When sintering occurs in a powder mixture, the two factors dominating are physical and chemical interactions between the particles. These factors dominate during the different events of sintering, physical interaction is dominant during the initial stage of sintering and the chemical interaction occurs later during the process of sintering [German(2014)]. During sintering of the powder mixtures with the different melting points, the powder with the lower melting point tends to melt and surrounds the solid particle of the higher melting point. The sintering that occurs in the melt is called liquid phase sintering, which in turn increases the sintering rate [German(1996)].

2.5.2 Liquid phase sintering

Liquid phase sintering (LPS) occurs when one phase has a lower melting point. As a result, the liquid melt is formed at the melting temperature of one of the materials, which surrounds the solid particles of higher melting point. In most cases, the solid particles are soluble in the liquid melt. As a result, capillary forces drive the attraction between the particles, along with which the solid particles get softened because of the high temperature, which results in densification. The presence of the liquid surrounding the solid particles results in higher diffusion rates and further in faster sintering at a lower temperature. LPS is mainly the dominant type of sintering with mixed powders and is also present in some alloy powders [German et al.(2009)German, Suri, and Park].
During LPS, there are three stages to attain full densification :

- Rearrangement of particles
- Solution-reprecipitation
- Final stage sintering

As the liquid forms between the solid particles, rearrangement of particles will occur. After the rearrangement stage is declining towards the end, solution-reprecipitation begins during which grain growth and grain shape accommodation occurs because of solid solubility and diffusivity rates. During the last stage of LPS, it is the densification of the solid structure formed from the previous stage. Therefore, densification is comparatively slower because of the formation of rigid structures between the grains [German(1996)].

2.6 State-of-the-art on synthesis of $TiAl/Al_2O_3$ by processing TiO_2 and Al

There are a number of studies focused on synthesising intermetallics of Ti using reinforcing particles such as Al_2O_3. For example, the research work done by [Binh(2021)] using initial powders of TiO_2 (2μm) and Al (<50μm) to produce a composite of Ti_3Al and Al_2O_3. They ball milled the powders for 8 hours at 300 rpm in Ar atmosphere and compressed into pellets at a pressure of 100 MPa. The study also comprises information regarding heat treatment of the material. Al_3Ti forms because of the reaction between Al and TiO_2 at temperature >800 ° C, the formation of alumina occurs above 800 ° C and the α Ti(Al, O) forms at a temperature above 1000 ° C according to [Ying(2004)] shared by [Binh(2021)]. An exothermic peak at temperature close to 600 ° C was found [Binh(2021)]. The first exothermic peak has been proposed to be the reaction between Al and TiO_2 powder [Binh(2021)]. This study gave an understanding on the reaction that will occur with temperature.

The atmosphere used for synthesis can influence TiO_2 when the intrinsic defects in the TiO_2 crystal structure is occupied by H_2 atoms. Since intrinsic defects play a significant role in sintering [Burg(2007)], the atmosphere of H_2 during synthesis can influence the resulting powder composite.

A study by [Schaffer and Hall(2002)] about the influence of the atmosphere while sintering Al nanopowders found that Al gained weight while sintering in the atmosphere of nitrogen (N_2) compared to Ar where the mass gain has been constant. Therefore, the effect of the atmosphere is found to influence the final properties of the resulting material [Schaffer and Hall(2002)].
The effect of the atmosphere on TiO_2 during synthesis studied by [Labus and et.al.(2014)] found that, weight loss is observed during the synthesis, this depending on the type of atmosphere. Also, the phase change from anatase to rutile was found to be delayed by a narrow temperature range when using N_2 instead of air during synthesis [Labus and et.al.(2014)]. Since anatase is a more reactive phase than rutile [Pan and et.al.(1997)], the delay because of difference in the atmosphere may result in a better sintering rate.

The formation of $TiAl/Al_2O_3$ is a result of reaction between Al and TiO_2 particles during synthesis. The formation of the intermetallic ceramic composite powder takes place in a series of reactions that occurs at low temperature (close to 660 °C) and another at high temperature (close to 1200 °C) [Ying(2004)]. During the low-temperature reaction- close to the melting point of Al, the first reaction occurs between the interface of Al and TiO_2 resulting in Al_3Ti. Since Al_3Ti has the lowest driving force, this compound forms even with 0.5 % Ti, being the first component that forms. During the reaction, liquid Al could surround the TiO_2 particles. However, the Ti particles diffuse into Al causing the formation of Al_3Ti, which is of a higher melting point, hence the material remains as solid particles in the system. In the study by [Ying(2004)], it has been proposed that Al_3Ti particles are surrounded by TiO_2. Since the diffusivity of Ti and Al into TiO_2 through Al_3Ti is low, they pose a barrier to the reaction that results in $TiAl/Al_2O_3$. Hence for this reaction to occur, the sintering temperature is to be higher than 820 °C - 920 °C [Ying(2004)]. Thereby, it is necessary to synthesise at temperatures greater than 920 °C.

Another product of this reaction is Al_2O_3, which forms during the low-temperature reaction. Sintering at high temperatures results in the phase transformation, during which transformation from amorphous oxide into γ-Al_2O_3 occurs. This phase transformation results in a thin oxide layer with local discontinuities. These discontinuities accelerates oxide layer growth and forms a continuous γ-Al_2O_3 layer. As the temperature increases further, growth γ-Al_2O_3 layers occur until crystallites of α-Al_2O_3 forms [Ying(2004), Trunov and et.al.(2006)].

3
Methods

3.1 Characterisation techniques

This section explains the characterisation techniques and their principles used in the research study which results are summarised in this report. The aim of characterising the synthesised material is to validate the selection of processing parameters to obtain the desired compounds. The morphology of the powder, phases present before and after synthesis, chemical composition and tracking of the synthesis process was carried out by scanning electron microscopy (SEM), light optical microscopy (LOM), x-ray diffraction (XRD), energy dispersive spectroscopy (EDS), oxygen analysis by inert gas fusion and thermogravimetric analysis (TGA).

3.1.1 Scanning electron microscopy (SEM)

SEM is mainly used for the examination and analysis of microstructure of a material and powder morphology. It has widely been an instrument of application in powder metallurgy because of its versatility, such as analysing the surface characteristics of the powder particles and also chemical contrast on the area of focus. It operates on the principle of light optics with an electron beam source [Aharinejad and Lametschwandtner(1992), Hirschhorn and Roll(1970)].

It uses a beam of electrons that passes through a set of electromagnetic lenses, which focuses the beam on the sample. The primary electrons bombard the specimen and scatters as backscattered electrons (BSE), secondary electrons (SE), and characteristic x-rays, these signals are used to analyse the morphology and chemical composition of the sample [Aharinejad and Lametschwandtner(1992)], [Hirschhorn and Roll(1970)]. These electrons are collected by the detectors to get an image of the focused area. The image from the SEM results from information obtained pixel by pixel throughout the desired area.

When electrons bombard the surface, elastic and inelastic scattering occurs. Elastic scattering can be defined as the scattering that occurs without a change in energy. Inelastic scattering can be defined as the scattering that is accompanied by the change in energy. This difference in energy from inelastic scattering depends on the energy of the incoming electron and the binding energy of the electrons in the sample's atom. Besides SE and BSE, there are other signals that are emitted, such as auger electrons, x-rays, and cathodoluminescence [Zhou(2006)].
When the SE are released because of an electron beam striking the sample, it releases

the loosely bound electrons from the sample that gives the topography. With the BSE signal, contrast is achieved based on the atomic number of the element. An element of a higher atomic number will possess a greater number of protons in the nucleus. Hence, there is more scattering of electrons, which results in a brighter image, achieving a higher contrast [Zhou(2006)].

3.1.2 Light optical microscopy (LOM)

LOM is a technique used to observe the topography of the sample. The principle of LOM involves light transmission and reflection, while transmission is the beam of light focused on the sample, reflection is the light that bounces back from the sample [Ebnesajjad(2011)]. It can create a magnified image of the sample under observation with an objective lens by the adjustment of an eye piece and magnification [Ebnesajjad(2011)].

The sample topography can be observed, which can reveal information such as the porosity, inclusions, type of fracture, corrosion, and cracks. If the metal samples are etched with a suitable etchant, it can also reveal the microstructural appearance [Ebnesajjad(2011)].

3.1.3 X-ray diffraction (XRD)

XRD is a non-destructive characterisation technique used to get information on the phases, crystallographic structure, residual stress, and chemical properties of the materials.

The XRD system consists mainly of an x-ray source, optics, a 2D detector, a sample stage and a monitor. It also requires a software with integrated database to analyse the data obtained from the measurement. With an XRD system it is possible to attain diffraction patterns simultaneously in two-dimensional space and analyse the data from the scanned area [He and Preckwinkel(2000)].

When the x-ray beam makes contact with the sample, these are diffracted by the single crystal point in individual directions, each of the directions from different diffraction planes. When a polycrystalline sample is analysed by XRD, the diffracted cones form from a particular family of crystallographic planes [He and Preckwinkel(2000)].

The parallel planes of atoms with interplanar distance ‘d’ results in constructive interference, this only occurs when Bragg’s law is satisfied. As the x-ray beam interacts with atoms, scattering occurs which produces a diffraction pattern. These diffraction patterns are identical to individual phases, which reveals the phase composition of the sample.

3.1.4 Chemical analysis

3.1.4.1 Energy dispersive spectroscopy (EDS)

EDS is a characterisation technique used for the identification of elements in a sample by an additional detector in the SEM equipment. The technique is capable of detecting elements with atomic numbers greater than boron and with a composition of at least 0.1%. EDS is chosen for material identification which gives elemental composition, spot analysis on the region limiting to a diameter of 10 μm [Abd Mutalib and et.al.(2017)].

The EDS works on the principle that utilises the electron beam released by the electron gun in the SEM instrument. As the electron beam interacts with the sample, it emits an x-ray that is unique to the particular element [Abd Mutalib and et.al.(2017)]. When the electron beam bombards an atom it results in the ejection of an electron leaving behind an electron-hole. Due to the presence of a hole, the electron from the outer shell will occupy the hole. Since the electron from the outer shell has a higher energy, the electron that occupies the inner shell will emit x-rays due to the energy difference between the shells. The x-ray emitted consists of an x-ray continuum and characteristic x-ray. The x-ray continuum is generated as a result of deceleration of electrons which provides the elemental composition of the sample under analysis. The characteristic x-ray is generated due to the occupancy of an electron from the outermost shell to the inner shell [Abd Mutalib and et.al.(2017)].

3.1.4.2 Inert gas fusion

Inert gas fusion provides a quantitative estimation of chemical elements such as hydrogen, nitrogen and oxygen in the materials [Fricioni and Essig(1986)]. The inert gas fusion technique uses a graphite crucible which is inserted in an impulse fusion furnace along with the sample. A current of 600 - 1300 A applied to the graphite crucible heats the crucible to a temperature of 3000 °C by the process of induction heating. The graphite crucible also acts as a source of carbon which combines with oxygen as it gets released. As the bond between the C and O forms, any further reactions are isolated [Fricioni and Essig(1986)].

For oxygen analysis, the samples are more prone to contamination. Any oxygen present in the system will increase the oxygen content of the sample. Hence the powder samples to be analysed require extended flushing after the sample is transferred into the crucible to remove any oxygen that can be present in between the powder particles [Fricioni and Essig(1986)].

3.1.5 Thermal analysis

3.1.5.1 Thermogravimetric analysis (TGA)

TGA measures the change in mass of the sample based on temperature and time variations in a controlled atmosphere with a defined heating and cooling rate. It allows determining the material's stability in different atmospheres.

The instrument works on the principle of variation in weight of the sample that undergoes mass change as a result of sample interaction with processing atmosphere or decomposition. The variation of weight in the sample is measured by a microbalance in the system. The system consists of a sample pan onto which a sample is inserted and is in contact with a thermocouple in order to accurately measure the change in temperature. The temperature, heating and cooling rate in the system is fixed per measurement and selected by the user depending on the experimental requirements [De Blasio(2019)].

3.1.5.2 Simultaneous thermal analysis (STA)

STA presented in Figure 3.1 enables to perform thermogravimetry (TG) and differential scanning calorimetry (DSC) analysis using the same instrument with different setups for the thermocouple and crucible installation. The merits of using STA is that it is time effective, and allows comparison in TG and DSC results simultaneously in the same conditions of heat treatment.

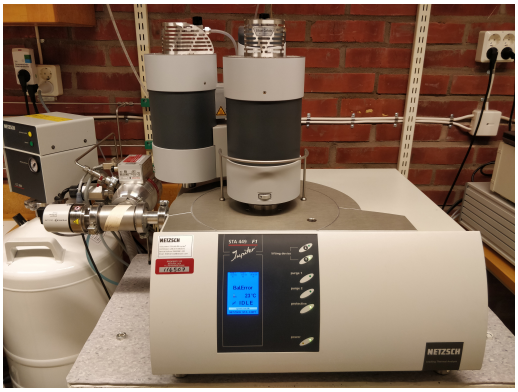

Figure 3.1: Simultaneous thermal analyser - STA 449 F1 jupiter used in this study

3.2 Experimental procedure

The Figure 3.2 is a brief visual representation of the experimental procedure followed for research during this thesis project.

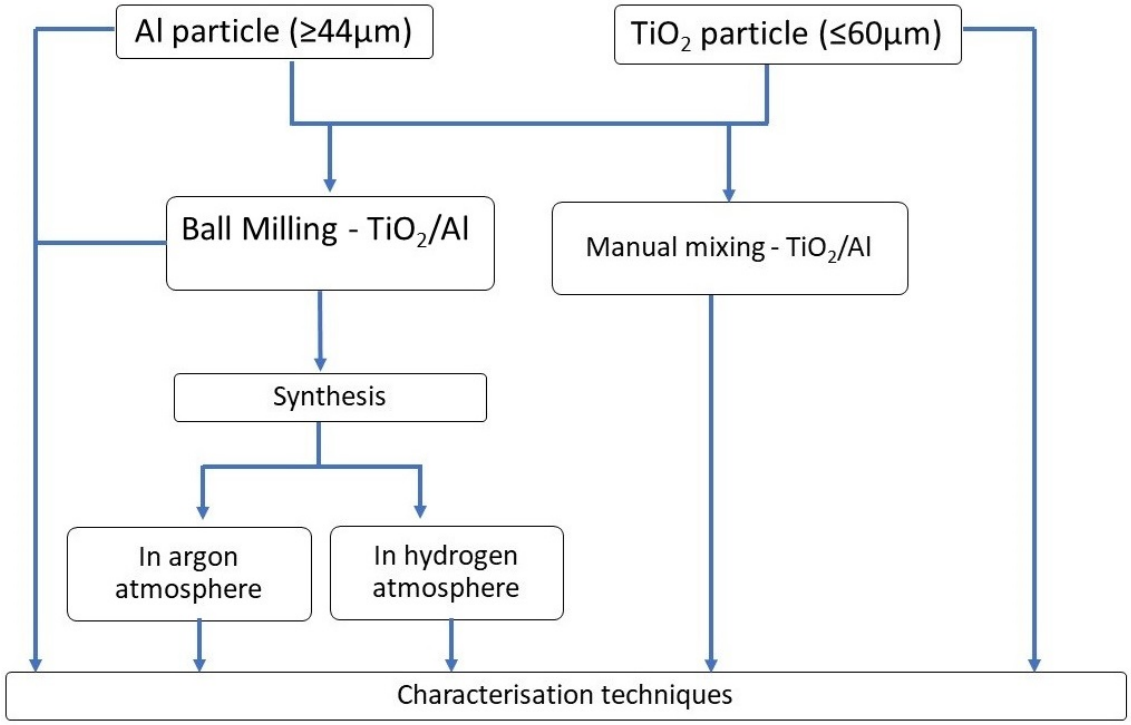

Figure 3.2: Workflow of experiments.

3.2.1 Powder properties

The raw powder, TiO_2 (anatase) with particle size larger than 44μm, purity of $\geq$ 99% and trace metal of $\leq$ 10000 ppm was procured from Sigma Aldrich. Al powder with maximum particle size of 60 μm, purity of 99.99% from the supplier Merck was used in this research.

3.2.2 Powder preparation

The powders were prepared, weighed and mixed based on the stoichiometric equation as follows:

$$3TiO_2 + 7Al \rightarrow 3TiAl + 2Al_2O_3$$

The powders were ball milled following the ratio, weight of the powder to the weight of the balls (1:2). Following this ratio, the powder along with combination of small and large ceramic balls were weighed and transferred to the ceramic crucible. The process was carried out in an Mbraun lab master 130 glove box following the safety procedures while handling powders.
The powders were further processed with the Pulverisette 7 classic line ball milling machine (Figure 3.3).

3.2.3 Ball milling

Ball milling was chosen for mixing the feedstock powders. In order to avoid cross contamination, the powders were ball milled in Pulverisette 7 classical line which uses ceramic crucibles and balls (Figure 3.3).

Considering the amount of powder the crucible can hold, the powder weight was measured following the stoichiometric equation to be 1 gram of Al and 1.25 grams of TiO_2, 4.5 grams of ceramic balls were inserted into the crucible which was prepared in the glove box.

The ball milling was performed at 100 rpm for 30 minutes at an interval of 5 minutes every 10 minutes to avoid any heating during continuous working of the apparatus. The powder preparation was carried out at a room temperature range of 23 - 25 °C and humidity were in the range of 10 - 25 %. Before the preparation, optimisation of the ball milling parameters were done using different time intervals from 10 - 30 minutes, in which 30 minutes proved to be the optimal period for full mixing of the powder.

The powder after ball milling was taken into the glove box and then transferred to a storage container. It was observed that a layer of the powder was present on the inner area of the crucible as a result of TiO_2 smearing.

Figure 3.3: Pulverisitte 7 classical line used in this study.

3.2.4 Microstructure characterisation

The sample preparation was done with a double side carbon tape pasted on a pin, powders were transferred to the tape on which they attach and blown with pressured air to remove the loose powder particles.

For the SEM analysis, the accelerating voltage of 5 kV was used for imaging and 15 kV was used for compositional analysis, depending on the purpose of the measurement. The powders were inspected with Philips XL 30 ESEM (Figure 3.4) using SE and image was obtained from Scandium software. The powder's morphology was observed by SEM.

The element composition analysis was done using EDS, INCA X-sight detector with BSE. The EDS analysis was done at a working distance of 8 mm. For this measurement, the accelerating voltage was increased to 15 kV. The scan speed of the analysis and precision time was increased for higher resolution. The expected elements were selected and EDS analysis was performed with software INCA analysis to obtain the elemental distribution map.

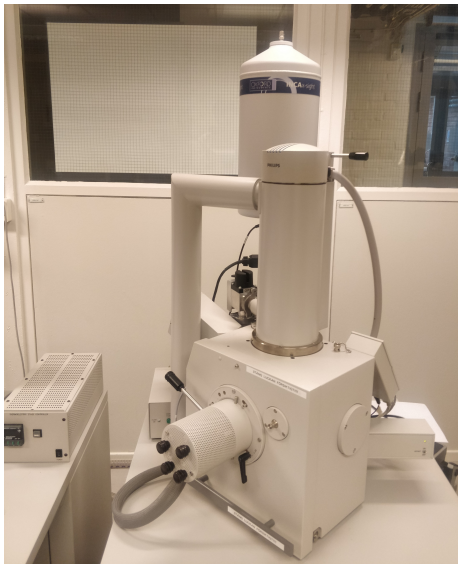

Figure 3.4: Philips XL 30 ESEM used in this study.

3.2.5 Synthesis of ball milled powder

The ball milled powder was synthesised in the presence of argon (Ar) atmosphere, since it is an inert gas. Also, hydrogen (H_2) atmosphere was used to understand the influence of H_2 as a reducing agent during synthesis. For the synthesis, the ball milled powder was placed on a crucible inside the system and the parameters for synthesis were set to a temperature from 25°C to 1200°C at 10 °C/min and a dwell of two hours at 1200°C both in Ar and H_2 atmospheres.
TG analysis was used in this study for synthesis and to understand the materials stability with temperature and atmospheres of Ar and H_2. TG analysis was done using the instrument in Figure 3.1. For the analysis, the weight of the empty crucible

and weight of the powder was measured which was later added as parameters into the software. The crucible with the powder was measured and placed on the thermocouple sensor. The silicon carbide furnace was chosen for a temperature range of 25 °C - 1550 °C.

Approximately 1.2 g of ball milled powder mixture were transferred to an alumina crucible. The crucible was then loaded into the instrument (Figure 3.1), which was then evacuated of any air residues with vacuum and then flushed with Ar (99.99%) three times to assure the purity of the synthesis atmosphere during the experiment. Following the experimental preparation, the parameters for the synthesis were inserted into the software and the atmosphere of Ar or H_2 was chosen.

To reduce the influence of noise and inaccuracies of the measurement, a calibration test was done with 1.2 grams of filler using alumina with same parameters as the synthesis. Later, the resulting calibration curves and the TG curves for ball milled powder synthesised in Ar and H_2 atmospheres were subtracted resulting in the final TG curves presented in this report.

3.2.6 Powder cross-section preparation

The samples of ball milled powder, ball milled powder synthesised in Ar and H_2 atmospheres were prepared to study the effect of atmosphere in the internal structure of the particles. For the sample preparation, Viafix molding, a cold mounting resin was used. Cold mounting is chosen to prevent the influence of heat and pressure during hot mounting that can change the microstructure of low temperature metals such as Al.

For the sample preparation, a copper ring was used to fix the powder. Viafix was prepared with 22 grams of powder and 18 grams of liquid, which was stirred for 30-40 seconds until the powders were homogeneously mixed. The resin was later transferred into the mold and hardened for 30-40 minutes.
After which, the sample was grinded and polished using a manual grinding and automatic polishing machines, Struers labopol-21 and Struers tegrapol-31, respectively (Figure 3.5). The parameters listed in Table 3.1 were followed for the preparation.

Table 3.1: The polishing methodology and parameters followed for the preparation of powder cross-section.

Speed [rpm]	Time [min]	Force [N]	Rotation	Lubricant	Grit/polishing cloth
100/150	3	10	↻↻	Water	2000
100/150	2	10	↻↻	DiaPro Dac 3μm	MD-Dac
100/150	1	10	↻↻	DiaPro Nap 1 μm	MD-Nap

Figure 3.5: Manual grinding machine: Struers Labopol-21 (left) and automatic polisher: Struers Tegrapol-31 (right) used in this study.

3.2.7 Light optical microscopy

LOM was the choice of instrument to observe the quality of powder cross-section prepared before SEM analysis was done.

The microscope used for the analysis during the project was Zeiss Axioscope 7. The sample was placed and observed on the motorized X-Y table using a magnification range between 10 and 50 X with Zeiss Axiocam 105 colour camera and operated using Zen core 2.7 software.

3.2.8 Gold sputtering

For the powder cross-section preparation, cold mounting of the powder was done using a non-conductive resin - Viafix. A non-conductive resin would result in accumulation of charges during SEM imaging, therefore, a layer of gold was sputtered on top to make the sample conductive and reduce the charging effect.

3.2.9 Oxygen analysis

Oxygen analysis was done to analyse the fraction of oxygen element present. The powders were deposited in a graphite crucible and heated up to 3000 °C. For this measurement, four sets of powder samples were prepared:

- Manual mixed TiO_2 and Al - the powders of TiO_2 and Al were mixed following the stoichiometric equation.
- Ball milled TiO_2 and Al powder.
- Ball milled powder synthesised in Ar atmosphere.
- Ball milled powder synthesised in H_2 atmosphere.

The bulk contents of oxygen from the samples were analysed using inert gas fusion LECO instrument TC-600 at Höganäs AB.

3.2.10 XRD analysis

The manual mixed, ball milled and synthesised powders were characterised using XRD to understand the phase transformation from TiO_2 and Al to TiAl and Al_2O_3. The same four sets of powder described in previous section (3.2.10) were used.

The XRD analysis was done with a Cu source. The 2θ ranges from 10° to 120° to capture most of the phases present in the sample. The peaks were indexed using X'Pert HighScore Plus and graphs were plotted using Origin.

4

Results & Discussions

4.1 Initial powder particles morphology

The SEM image of TiO_2 (Figure 4.1 a) shows blocky and coarse powder particles. The SEM image of Al particles (Figure 4.1 b) shows irregular morphology and coarse powder particles. The approximate particle size for finer particles of TiO_2 is in the range of 40 - 100 μm, while coarser particles within the range of 150 - 200 μm may have formed due to agglomeration of TiO_2 powder. Al particle size is in the range of 20 - 50 μm. The particle size was calculated using Image J software.

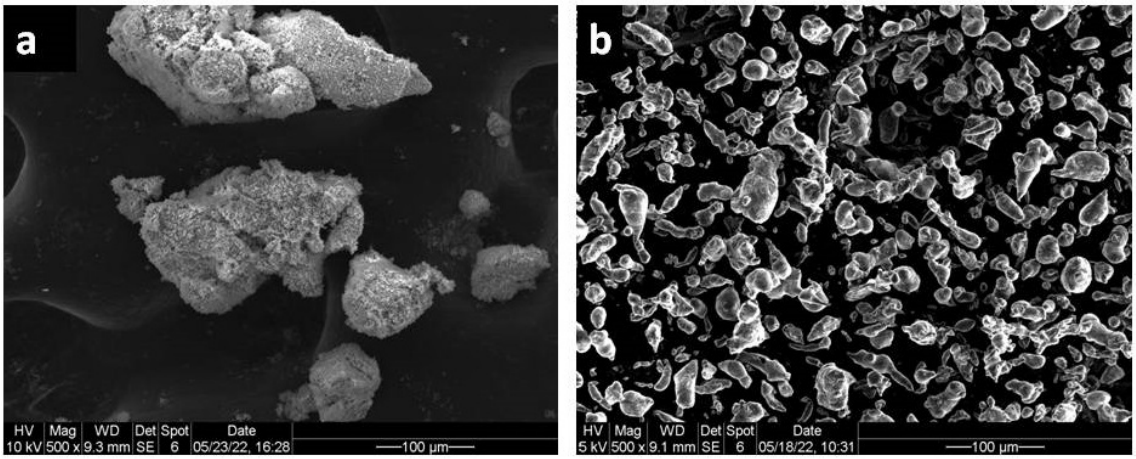

Figure 4.1: SEM images of a) TiO_2 powder particles and b) Al powder particles.

4.2 Particles morphology after ball milling

The ball milling process resulted in proper mixing and deformation of powder particles. Because of the mix between Al and TiO_2, a ductile-brittle particle combination will be expected. In fact, coarsening of particles occurred, as can be observed in the SEM images of Figure 4.2. Few coarser and irregular particles were found to be of a different size compared to the rest of the particles. The average size of one of these coarser particles was measured using Image J software and found to be 166.51μm.

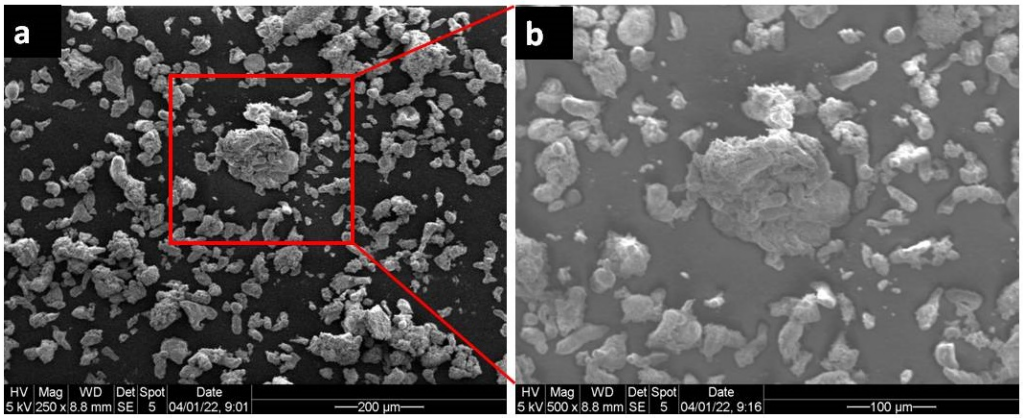

Figure 4.2: SEM image of TiO_2/Al powder, ball milled for 30 minutes at 100 rpm. a) Overview of the ball milled powder (marked area shows coarsened particle) and b) magnified image.

The EDS elemental map of the ball milled powder in Figure 4.3 shows that Al particles are attached to TiO_2. Hence, while referring to Figure 4.2 and Figure 4.3, it can be stated that coarser particles formed during ball milling were because of cold welding between Al and TiO_2 particles.

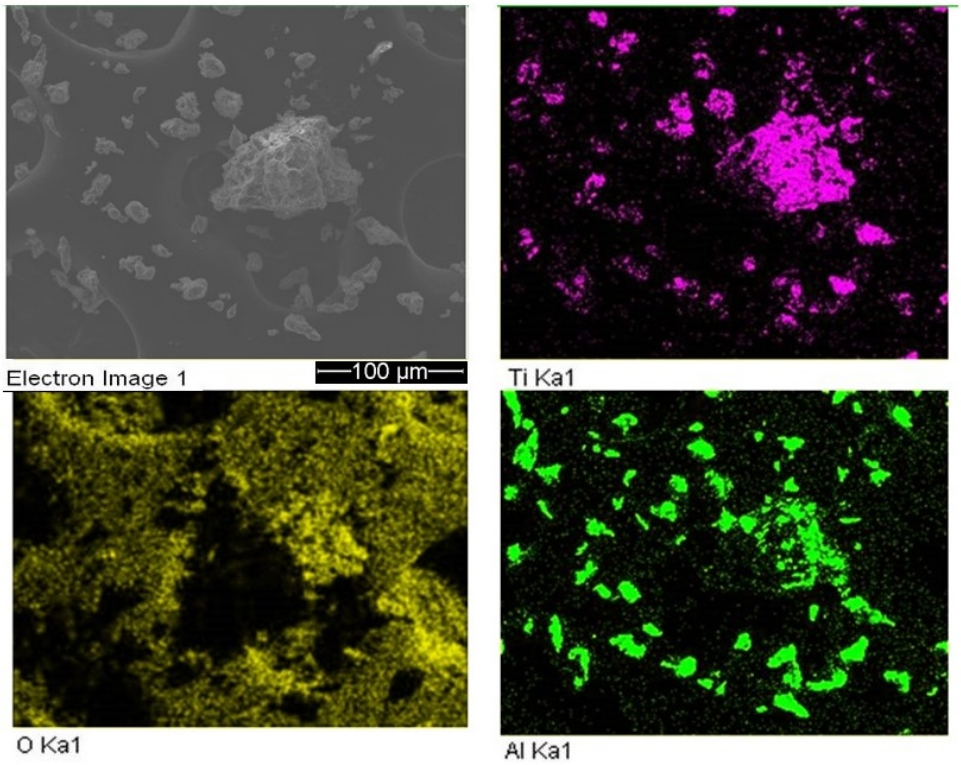

Figure 4.3: EDS elemental map of ball milled powder.

After ball milling, a layer of powder was present on the inner area of the crucible and ceramic balls because of the smearing property of TiO_2. Hence, the contamination during ball milling is reduced and life of the apparatus is not compromised. Additionally, the resulting powder showed a colour change from bright white (TiO_2) and dark grey (Al) powder feedstock to light greyish colour after ball milling, which could be an indication of well mixed TiO_2 and Al powders.

4.3 Visual inspection of ball milled powder before and after synthesis

The ball milled powder was synthesised from room temperature (25 °C) to 1200 °C and dwell for 2 hours at 1200 °C in Ar and H_2 atmospheres. It resulted in a change of colour from the initial light greyish to dark grey because of oxidation during the synthesis, as can be seen in the image of Figure 4.4.

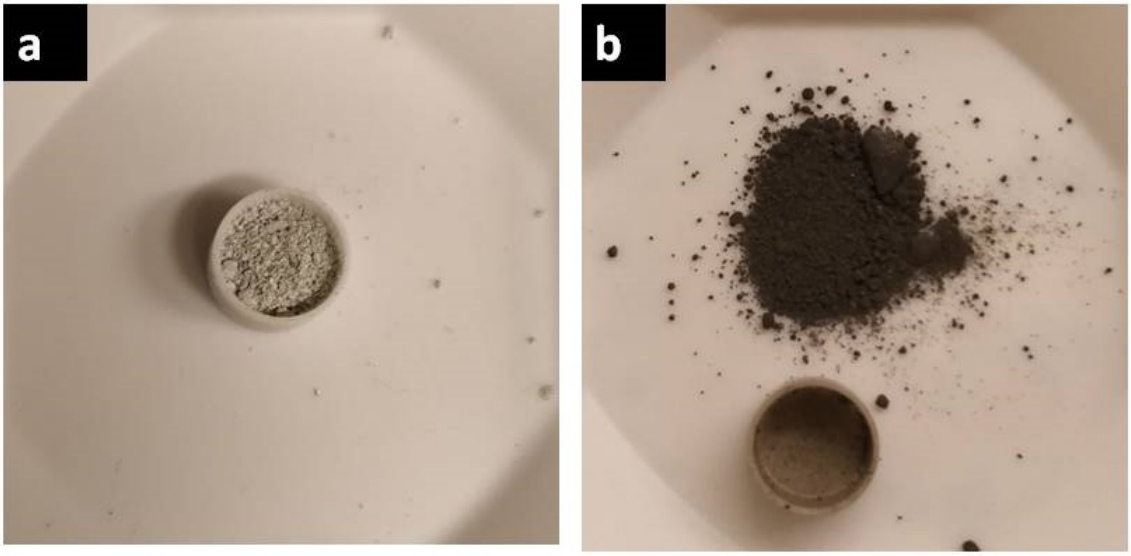

Figure 4.4: a) Ball milled powder, b) Ball milled powder after synthesis in Ar atmosphere.

4.4 Thermal analysis in argon and hydrogen atmospheres

The subtracted TG curve for synthesis in Ar atmosphere is shown in Figure 4.5. At the start, there is a drop in mass loss from room temperature until 400 °C. This mass loss happens most probably because of drying and/or desorption of physically or chemically bonded substances like water.

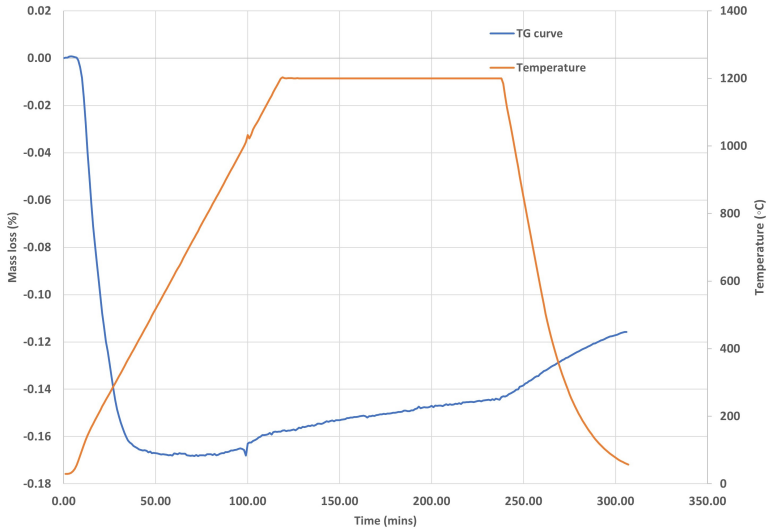

Figure 4.5: TG curve of ball milled powder during synthesis in Ar atmosphere.

The subtracted TG curve for the synthesis in H_2 atmosphere is presented in Figure 4.6. The initial drop in mass is also found here at the same temperature ranges, due to drying and/or desorption. The mass gain found during the dwell region can be due to the formation of titanium hydride (TiH_2) because, the formation of aluminium hydride (AlH_3) is difficult with conventional hydrogenation of Al [Wang et al.(2018)Wang, Rawal, Quadir, and Aguey-Zinsou].

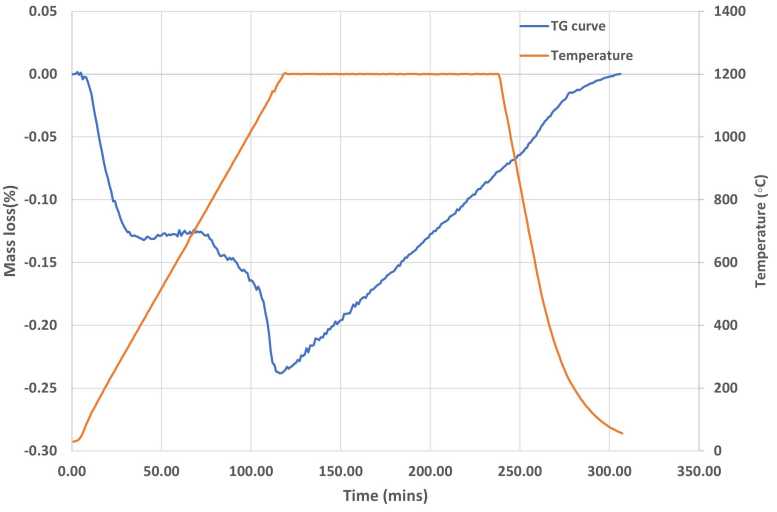

Figure 4.6: TG curve of ball milled powder during synthesis in H_2 atmosphere.

4.5 SEM analysis of synthesised powder

The ball milled powder synthesised in Ar atmosphere (Figure 4.7) comprises of few coarse particles around 100 μm and also other fine particles homogenously distributed. The coarsening seems to occur even more with ball milled powder synthesised in H_2 atmosphere compared to Ar, as shown in (Figure 4.8). This is also

verified by calculating the average particle size of the coarsened particles in H_2 and Ar atmosphere using Image J software to be 181.120 μm and 146.708 μm, even though the parameters of synthesis followed are the same as that of Ar atmosphere. When the coarsened particles in Ar and H_2 atmospheres were compared with ball milled powder (Figure 4.2), the synthesised particles have greater fraction of coarsened particles. This illustrates the influence of synthesis on coarsening of powder particles.

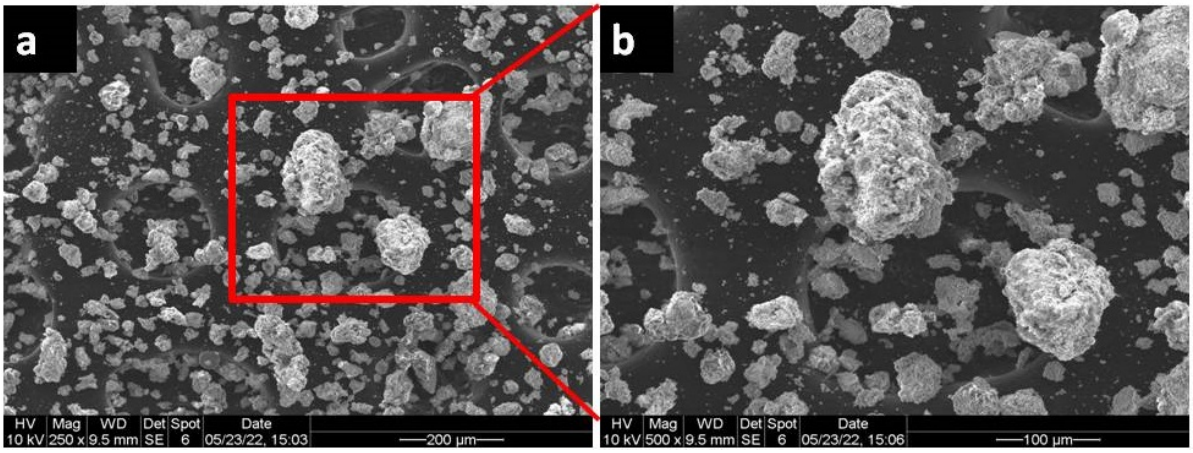

Figure 4.7: SEM image of ball milled powder synthesised in Ar atmosphere.

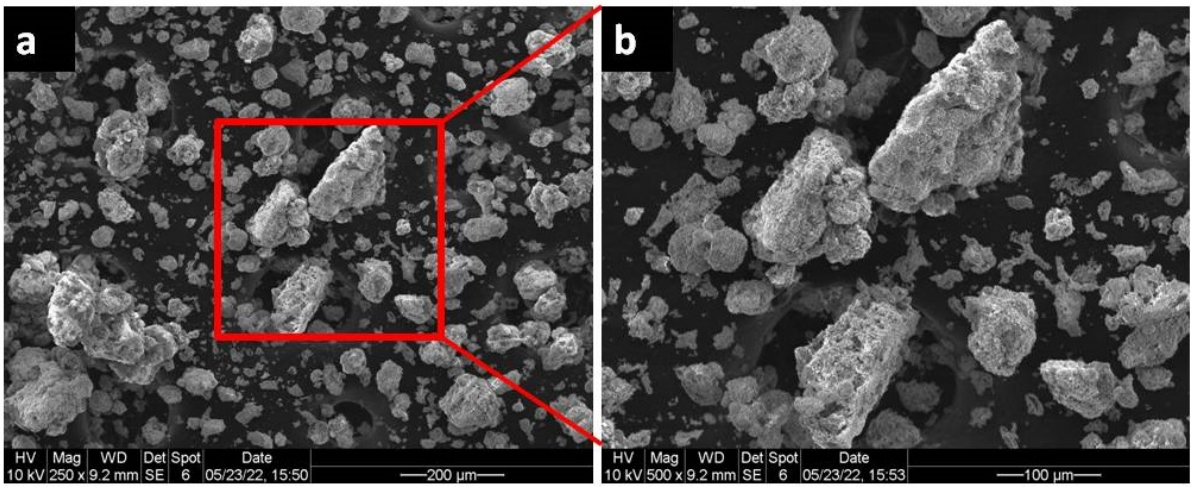

Figure 4.8: SEM image of ball milled powder synthesised in H_2 atmosphere.

4.6 EDS analysis of synthesised powder

The EDS elemental map analysis on an area of Figure 4.7 for ball milled powder synthesised in Ar atmosphere and an area of Figure 4.8 for ball milled powder synthesised in H_2 atmosphere was performed to analyse the distribution of elements. The EDS maps of ball milled powder synthesised in Ar atmosphere (Figure 4.9) and in H_2 atmosphere (Figure 4.10) shows that Al particles are not present as

separate particles as in Figure 4.3 for ball milled powder, but the maps show a good distribution of elements. Therefore, it was concluded that the synthesis resulted in a good distribution of elements, since three of the elemental maps Ti, O and Al showed homogeneity in the area of analysis. It was also found that areas with Ti, O, and Al overlap well with each other, this could be because of formation of the expected phases - $TiAl/Al_2O_3$. However, to confirm the formation $TiAl/Al_2O_3$, a detailed phase characterisation technique, XRD analysis was done, presented in section 4.10.

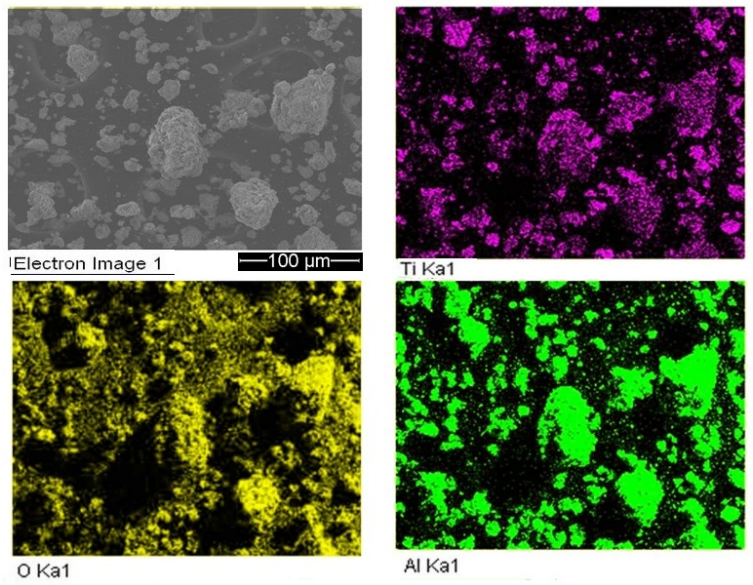

Figure 4.9: EDS elemental map of ball milled powder synthesised in Ar atmosphere.

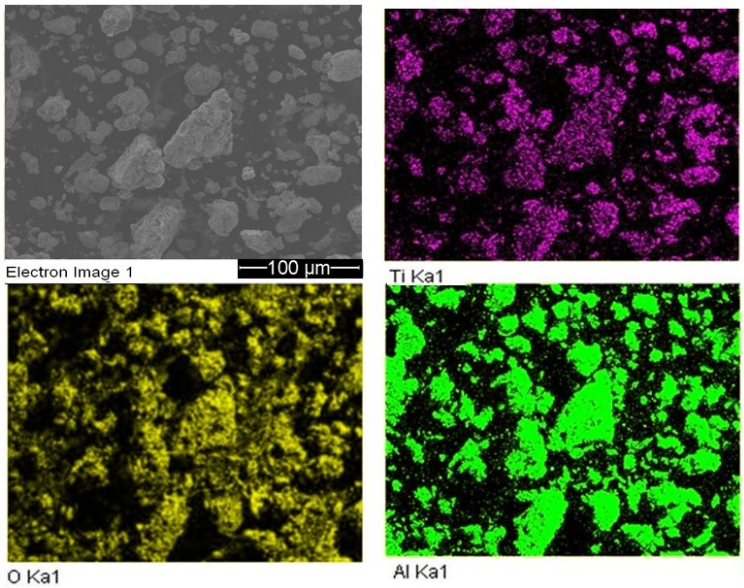

Figure 4.10: EDS elemental map of ball milled powder synthesised in H_2 atmosphere.

4.7 LOM of synthesised powder

The LOM image in Figure 4.11 shows the cross-section of ball milled powder. The LOM image for the cross-section of ball milled powder shows combination of two different particles in the cross-section. This combination of particles may have occurred because of the attachment of TiO_2 and Al particles. In order to analyse the morphology and confirm the elements present SEM-EDS analysis was done, which is further discussed in section 4.8.

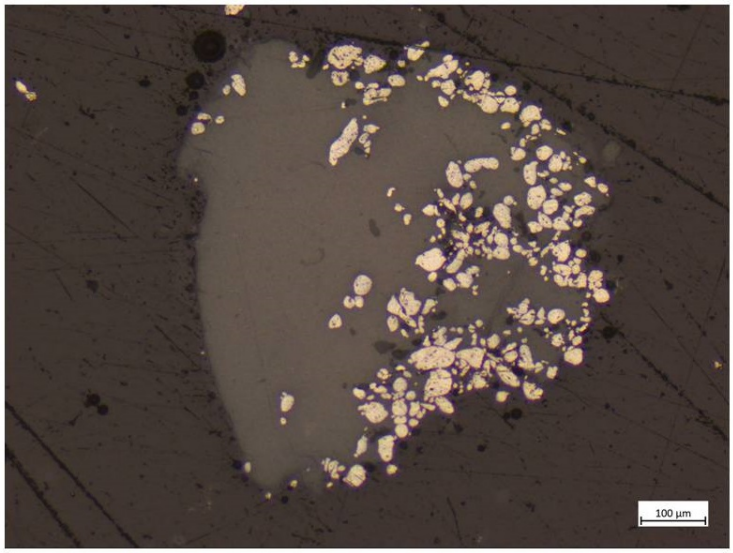

Figure 4.11: Powder cross-section LOM image of ball milled powder.

The LOM images in Figures 4.12 and 4.13 shows the powder cross-section with the features of ball milled powder particles synthesised in Ar and H_2 atmospheres. The LOM images of ball milled powder synthesised in Ar and H_2 atmospheres shows a sponge-like appearance in the cross-section. However, the fraction of sponge-like appearance seems to be greater for synthesised in H_2 atmosphere (Figure 4.13). In order to analyse the morphology with more detail, a more dedicated study using SEM was carried out and presented in section 4.8.

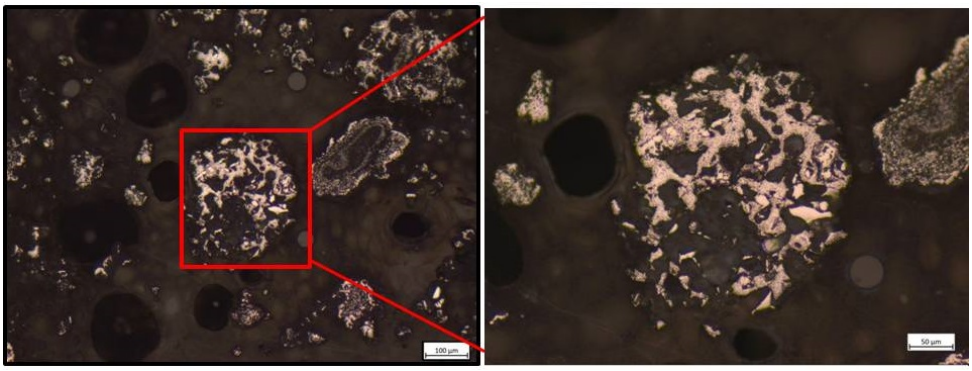

Figure 4.12: Powder cross-section LOM image of ball milled powder synthesised in Ar atmosphere.

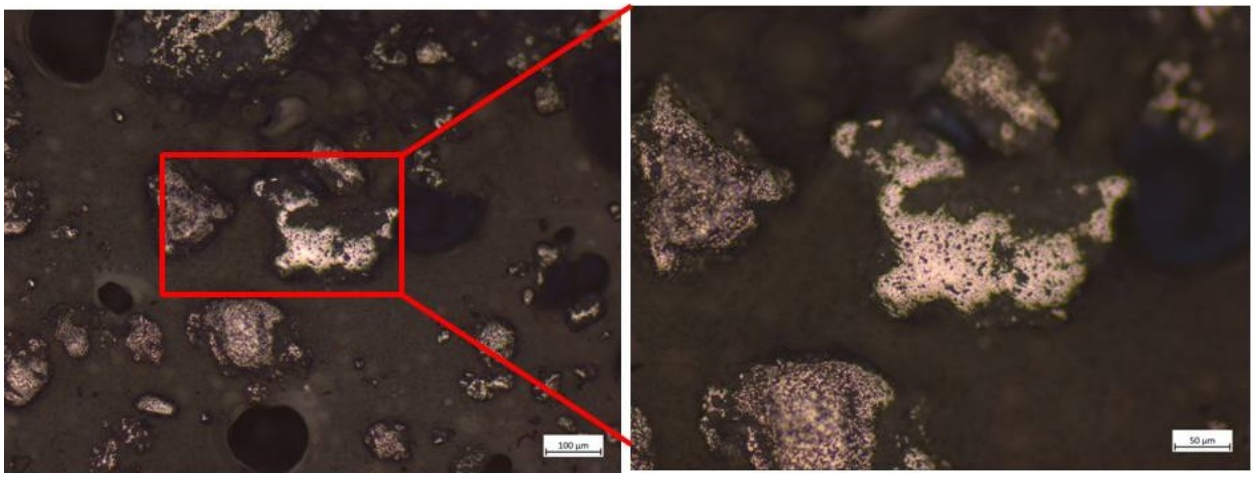

Figure 4.13: Powder cross-section LOM image of ball milled powder synthesised in H_2 atmosphere.

4.8 Powder cross-sections of ball milled and synthesised powder studied by SEM-EDS

The SEM image of the powder cross-section of ball milled powder (Figure 4.14) shows a difference in contrast in few particles, which can be because of attachment of Al particles to TiO_2 particles. This has been confirmed by EDS elemental map of ball milled powder (Figure 4.15). In fact, Al particles are attached to TiO_2 as observed in the cross-section because of the ductile property of Al, during the ball milling cold welding of Al and TiO_2.

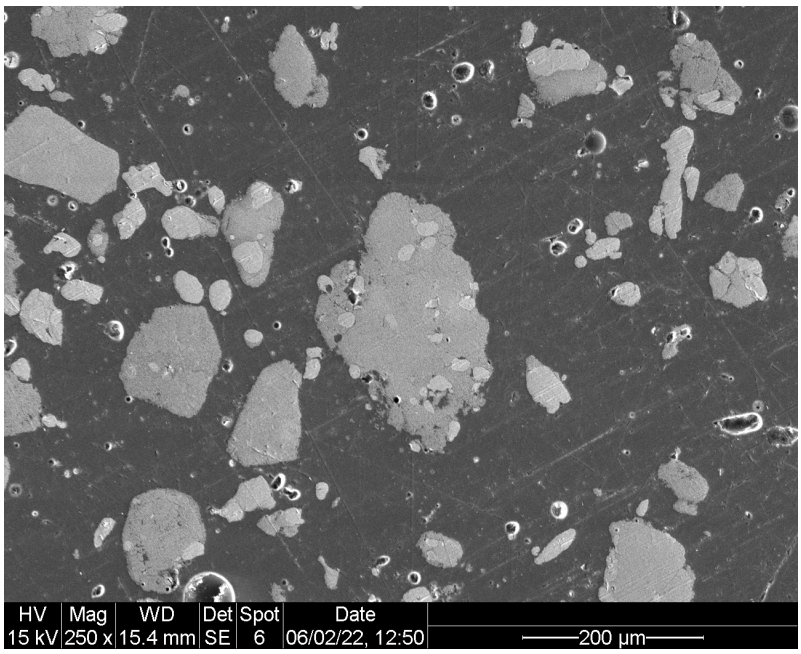

Figure 4.14: Powder cross-section SEM image of ball milled powder.

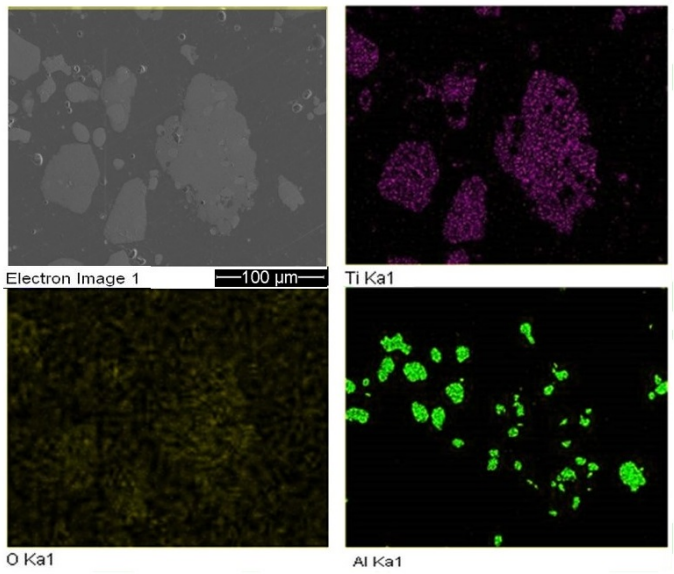

Figure 4.15: Powder cross-section EDS elemental map of ball milled powder.

As discussed in the previous section, presence of sponge-like morphology in the synthesised powder by Ar and H_2 atmospheres are confirmed. In fact, the SEM shows micro porosity in both the powder material, but it is more noticeable in the powder synthesised in H_2, while in Ar some parts of the particles show this morphology. One reason for such an appearance for synthesised in H_2 atmosphere can be because of the presence of an unexpected phase.

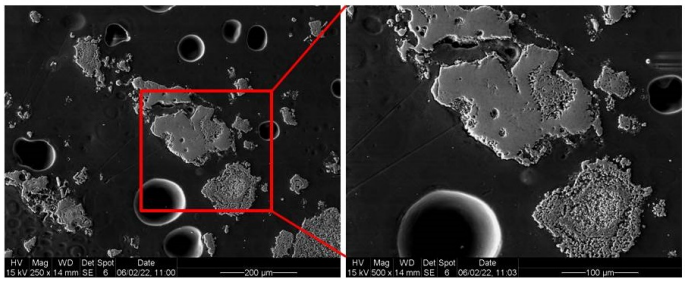

Figure 4.16: Powder cross-section SEM image of ball milled powder synthesised in Ar atmosphere.

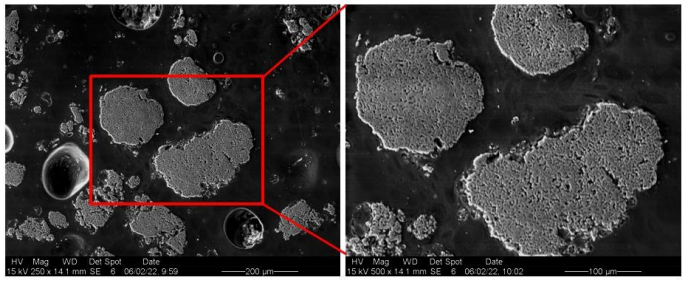

Figure 4.17: Powder cross-section SEM image of ball milled powder synthesised in H_2 atmosphere.

The EDS elemental maps of Ar atmosphere (Figure 4.18) and H_2 atmosphere (Figure 4.19), shows a homogeneous distribution of the elements Ti, Al and O. However, when observing the EDS quantitative results (Table 4.1), it was found that the O with Ar atmosphere is greater than with H_2 atmosphere. Whereas, the powder synthesised in H_2 atmosphere showed a greater % of Ti and Al elements. However, it is worth to mention that EDS is a semi-quantitative analysis. Trace elements such as oxygen cannot be accurately quantified. Therefore, oxygen analysis using inert gas fusion was carried out for comparison between the source powders, ball milled and synthesised powders, which is discussed in section 4.9.

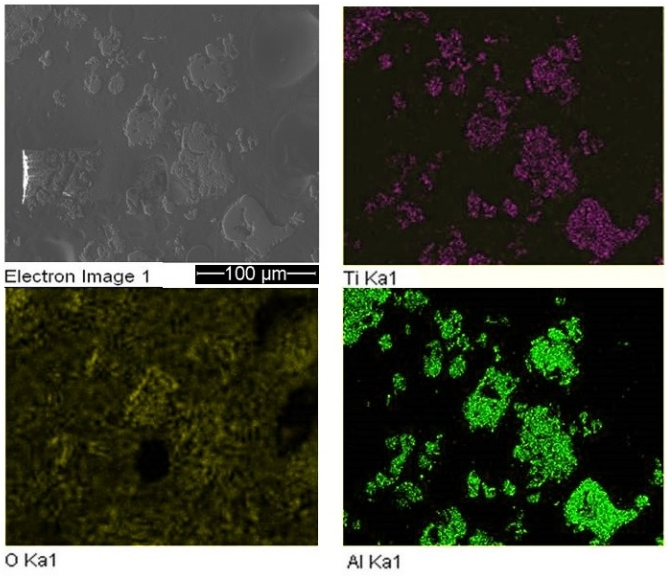

Figure 4.18: Powder cross-section EDS elemental map of ball milled powder synthesised in Ar atmosphere.

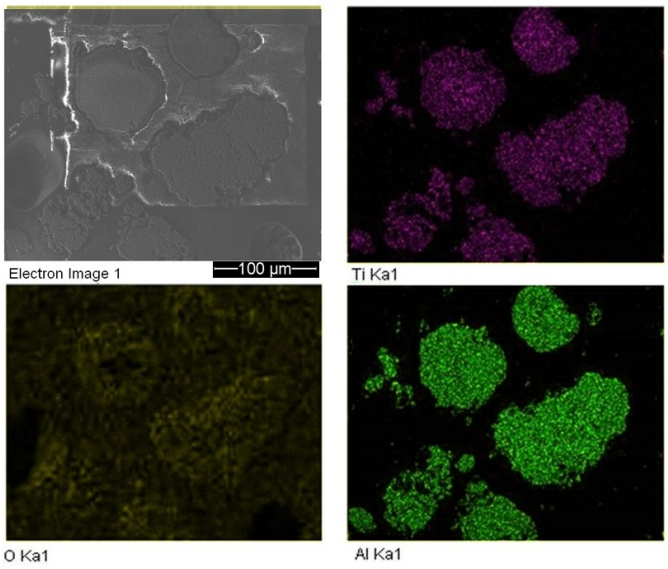

Figure 4.19: Powder cross-section EDS elemental map of ball milled powder synthesised in H_2 atmosphere

Table 4.1: EDS quantitative analysis (Figures (4.15, 4.18, 4.19)).

	Ball milled powder		Ball milled powder synthesised in argon		Ball milled powder synthesised in hydrogen	
Element	Weight (%)	Atomic(%)	Weight (%)	Atomic (%)	Weight (%)	Atomic (%)
O	46.31	64.23	58.27	72.42	51.62	67.30
Al	30.33	24.94	31.87	23.49	34.46	26.64
Ti	23.37	10.83	9.86	4.09	13.92	6.06
Total	100		100		100	

,

4.9 Oxygen analysis

The oxygen analysis by inert gas fusion gave the fraction of oxygen present in different samples. The analysis of the oxygen fractions are presented in the graph of Figure 4.20. The ball milled (BM) powder shows a higher oxygen content than manual mixed (MM) elemental powders. This was because the preparation of powder was not carried out under an inert atmosphere. Hence, the oxygen present inside the crucible could have contaminated the powder particles as they were deformed during the ball milling process.

Comparing the oxygen content of ball milled powder synthesised in Ar and H_2 atmospheres, Figure 4.20 shows that the oxygen content is the lowest for the powder synthesised in H_2 atmosphere. This can be because of the property of H_2 being a reducing agent.

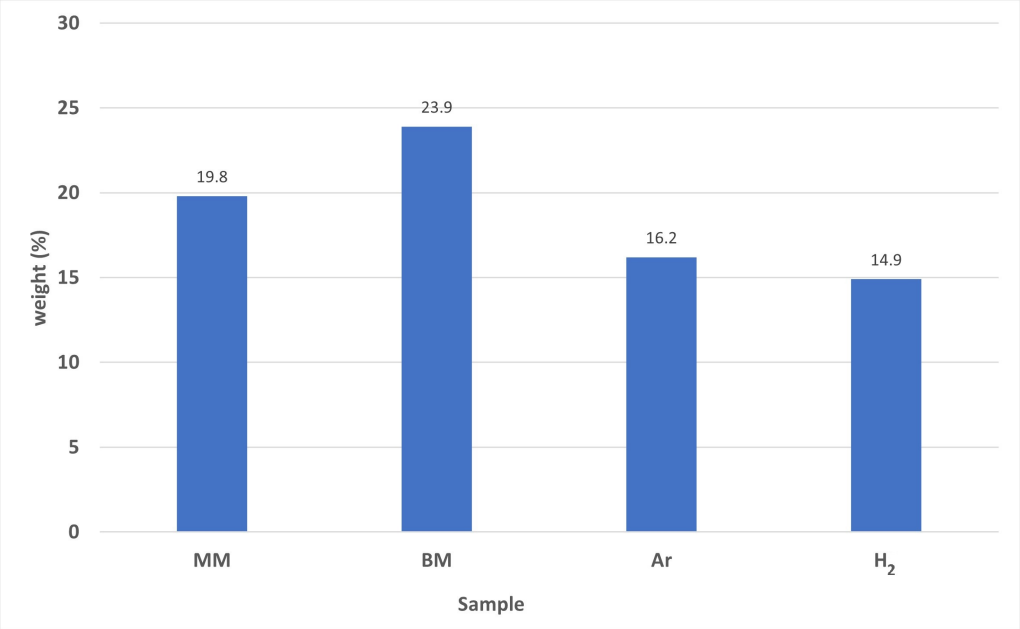

Figure 4.20: Oxygen analysis

4.10 XRD results

Following the study of the homogeneity of the powder chemical composition upon ball milling and synthesis processes. The powder phases distribution is analysed by XRD. This method allows to study the transformation from TiO_2 and Al to TiAl and Al_2O_3. The samples used for the XRD analysis have been labelled as follows:

- Manual mixed powder.
- Ball milled powder.
- Ball milled powder synthesised in Ar atmosphere.
- Ball milled powder synthesised in H_2 atmosphere.

The XRD results for manual mixed powder (Figure 4.21) and ball milled powder (Figure 4.22), shows the peaks of TiO_2 and Al. Hence it can be confirmed that the phases in the mixed powders, TiO_2 and Al are present.

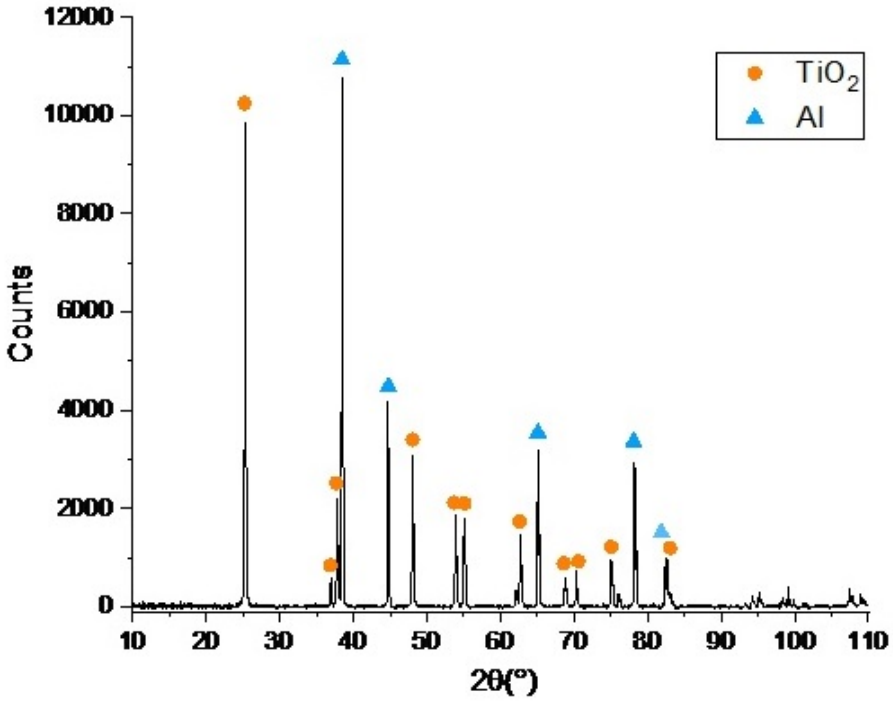

Figure 4.21: XRD peaks of manual mixed powder.

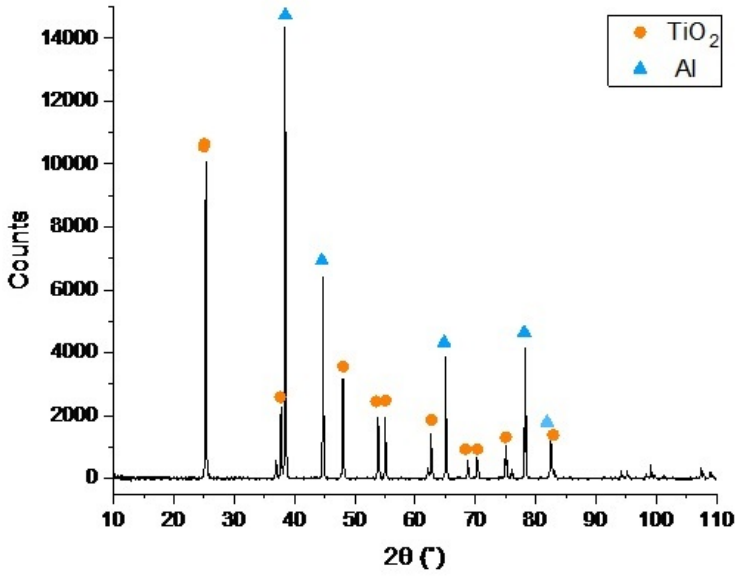

Figure 4.22: XRD peaks of ball milled powder.

The XRD results of ball milled powder synthesised in Ar and H_2 atmospheres are presented in Figure 4.23 and Figure 4.24. It was found that the XRD peaks of TiAl and Al_2O_3 were present for synthesised powders in both Ar and H_2 atmospheres, showing proof of a phase transformation from TiO_2 and Al to TiAl and Al_2O_3 during synthesis. As discussed in section 4.4 the possibility of TiH_2 presence as per the findings in the literature study for ball milled powder synthesised in H_2 atmosphere, this could not be validated by the XRD results (Figure 4.24). Since the XRD analysis shows only the peaks of TiAl and Al_2O_3 for synthesised in H_2 atmosphere, any other compound present in the powder is likely to be less than 5%, which is the detection limit of XRD.

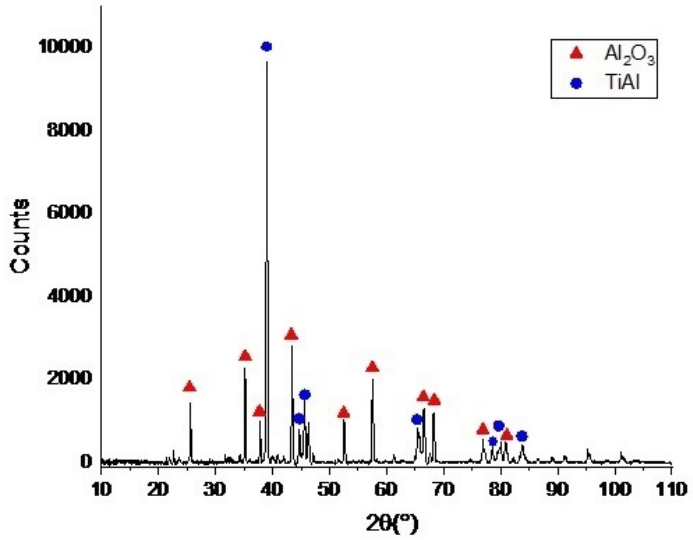

Figure 4.23: XRD peaks of ball milled powder synthesised in Ar atmosphere.

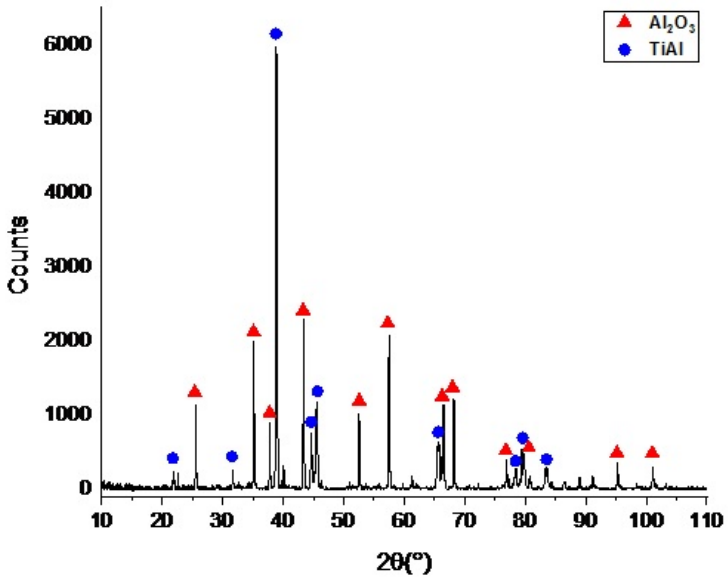

Figure 4.24: XRD peaks of ball milled powder synthesised in H_2 atmosphere.

5
Conclusions

The aim of the thesis project was to synthesise $TiAl/Al_2O_3$ compound from TiO_2 and Al powder using ball milling and study the phase transformation after synthesis. Therefore, some of the major conclusions drawn from the thesis project are:

1. The ball milling parameters (30 minutes and 100 rpm) for a complete mix of TiO_2 and Al were optimised, this was validated with the EDS elemental maps.

2. The powder cross-section analysis using both LOM and SEM reveals a slight difference in morphology of synthesised powder in H_2 atmosphere compared to Ar atmosphere. The fraction of sponge-like morphology is greater when synthesised in H_2 atmosphere.

3. The EDS elemental maps of ball milled powder synthesised in Ar and H_2 atmospheres shows homogenous distribution of Ti, Al and O elements. This homogenous distribution is because of the synthesis process that resulted in the formation of $TiAl/Al_2O_3$, which also agrees well with the XRD results.

4. Oxygen content was reduced in the powders synthesised in Ar and H_2 atmospheres compared to ball milled powder. A lower content of oxygen is present after synthesis in H_2 atmosphere as a result of H_2 being a reducing agent.

5. XRD analysis of manual mixed and ball milled powder shows peaks of TiO_2 and Al while the XRD spectra of ball milled powder synthesised in Ar and H_2 atmospheres consist of TiAl and Al_2O_3 peaks. This suggests the approach and parameters taken during the synthesis resulted in phase transformation from TiO_2 and Al to $TiAl/Al_2O_3$ to be successful.

6
Future work

Given the relevance of this research work for the surface coating industry for low-cost parts and aerospace industry, it is important to highlight the possibilities to broaden the scope of the results obtained in this master thesis:

1. Study the ability to scale up the production of powders with ball milling. Given the size of the vessels used for ball milling and the synthesis in TGA equipment, scaling up this approach will require a larger volume of start materials and equipments with higher capacity.

2. Processing of synthesised powder to flowable powder as a raw material for thermal spray coating. Each consolidation process requires different powder properties such as flowability and compressibility. Further characterising the powder taking into account these requirements would open more opportunities for consolidation.

3. DSC analysis to study the resultant reaction product in H_2 atmosphere. More details can be obtained on the reaction during synthesis with a deeper analysis using DSC equipment.

4. Investigate the effect of composition (TiAl and Al_2O_3 content) on properties such as corrosion resistance by using surface coating processing.

Bibliography

[Nakamura(1995)] Morihiko Nakamura. Fundamental properties of intermetallic compounds. *MRS Bulletin*, 20(8):33–39, 1995. URL https://doi.org/10.1557/S0883769400045085.

[Lütjering and Williams(2007)] Gerd Lütjering and James C Williams. Titanium based intermetallics, isbn=978-3-540-73036-1. *Titanium*, pages 337–366, 2007. URL https://doi.org/10.1007/978-3-540-73036-1_8.

[Binh(2021)] et.al Binh. Fabrication, microstructure, and microhardness at high temperature of in situ synthesized ti3al/al2o3 composites. *Metals*, 11(4):617, 2021. URL https://doi.org/10.3390/met11040617.

[Nissan et al.(2008)Nissan, Choi, and Cordingley] B Ben Nissan, AH Choi, and R Cordingley. Alumina ceramics. In *Bioceramics and their clinical applications*, pages 223–242. Elsevier, 2008. ISBN 978-1-84569-204-9. URL https://doi.org/10.1533/9781845694227.2.223.

[Ruys(2018)] Andrew John Ruys. *Alumina Ceramics: Biomedical and Clinical Applications*. Woodhead Publishing, 2018. ISBN 978-0-08-102442-3. URL https://doi.org/10.1016/C2017-0-01189-8.

[Taotao(2008)] Ai Taotao. Microstructure and mechanical properties of in-situ synthesized al_2o_3/tial composites. *Chinese Journal of Aeronautics*, 21(6):559–564, 2008. URL https://doi.org/10.1016/S1000-9361(08)60174-0.

[Froes(2015)] FHe Froes. *Titanium: physical metallurgy, processing, and applications*. ASM international, 2015. ISBN 978-1-62708-318-8. URL https://doi.org/10.31399/asm.tb.tpmpa.9781627083188.

[Kondoh(2015)] Katsuyoshi Kondoh. Titanium metal matrix composites by powder metallurgy (pm) routes. In *Titanium powder metallurgy*, pages 277–297. Elsevier, 2015. URL https://doi.org/10.1016/B978-0-12-800054-0.00016-2.

[Pan and et.al.(1997)] J. Pan and et.al. Microstructural study of the interface reaction between titania whiskers and aluminum. *Composites Science and Technology*, 57(3):319–325, 1997. ISSN 0266-3538. URL https://doi.org/10.1016/S0266-3538(96)00127-3.

[Diebold(2003)] Ulrike Diebold. The surface science of titanium dioxide. *Surface science reports*, 48(5-8):53–229, 2003. URL https://doi.org/10.1016/S0167-5729(02)00100-0.

[Chen and Li(2019)] Wei Chen and Zhiqiang Li. Additive manufacturing of titanium aluminides. In *Additive Manufacturing for the Aerospace Industry*, pages 235–263. Elsevier, 2019. URL https://doi.org/10.1016/B978-0-12-814062-8.00013-3.

[Liu and Liu(2015)] Bin Liu and Yong Liu. 27 - powder metallurgy titanium aluminide alloys. In Ma Qian and Francis H. (Sam) Froes, editors, *Titanium Powder Metallurgy*, pages 515–531. Butterworth-Heinemann, Boston, 2015. ISBN 978-0-12-800054-0. URL https://doi.org/10.1016/B978-0-12-800054-0.00027-7.

[Ivanova(2021)] et.al Ivanova. Study of the consolidation and phase formation in the γ-tial-based material sintered with a tih2 precursor. *Powder Metallurgy and Metal Ceramics*, 60(5):298–309, 2021. URL https://doi.org/10.1007/s11106-021-00240-2.

[Lumley(2010)] Roger Lumley. *Fundamentals of aluminium metallurgy: production, processing and applications*. Elsevier, 2010. ISBN 978-1-84569-654-2. URL https://doi.org/10.1016/C2016-0-02117-4.

[Chawla(2012)] Krishan K Chawla. Metal matrix composites. In *Composite materials*, pages 197–248. Springer, 2012. ISBN 978-0-387-74365-3. URL https://doi.org/10.1007/978-0-387-74365-3_6.

[Evans(2003)] et.al Evans. Metal matrix composites in industry. In *Metal Matrix Composites in Industry*, pages 9–38. Springer, 2003. ISBN 978-1-4615-0405-4. URL https://doi.org/10.1007/978-1-4615-0405-4.

[Suryanarayana(2001)] C. Suryanarayana. Mechanical alloying and milling. *Progress in Materials Science*, 46(1):1–184, 2001. ISSN 0079-6425. doi: https://doi.org/10.1016/S0079-6425(99)00010-9. URL https://doi.org/10.1016/S0079-6425(99)00010-9.

[German(2010)] RM German. Thermodynamics of sintering. In *Sintering of advanced materials*, pages 3–32. Elsevier, 2010. ISBN 978-1-84569-562-0. URL https://doi.org/10.1533/9781845699949.1.3.

[German(2014)] Randall M. German. Chapter eleven - mixed powders and composites. In Randall M. German, editor, *Sintering: from Empirical Observations to Scientific Principles*, pages 355–385. Butterworth-Heinemann, Boston, 2014. ISBN 978-0-12-401682-8. doi: https://doi.org/10.1016/B978-0-12-401682-8.00011-2. URL https://doi.org/10.1016/B978-0-12-401682-8.00011-2.

[German(1996)] Randall M German. *Sintering theory and practice*. 1996. ISBN 978-0-471-05786-4.

[German et al.(2009)German, Suri, and Park] Randall German, Pavan Suri, and Seong Jin Park. Liquid phase sintering. *Journal of materials science*, 44(1):1–39, 2009. URL https://doi.org/10.1007/s10853-008-3008-0.

[Ying(2004)] et.al. Ying, DY. Solid-state reactions during heating mechanically milled al/tio2 composite powders. *Metallurgical and Materials Transactions A*, 35(7):2115–2125, 2004. URL https://doi.org/10.1007/s11661-004-0160-2.

[Burg(2007)] et.al Burg. Effect of sintering on microstructure of tio2 ceramics. *Advances in applied ceramics*, 106(1-2):57–62, 2007. URL https://doi.org/10.1179/174367607X155981.

[Schaffer and Hall(2002)] G. B. Schaffer and B. J. Hall. The influence of the atmosphere on the sintering of aluminum. *Metallurgical and Materials Transactions A*, 33(10):3279–3284, October 2002. ISSN 1543-1940. URL https://doi.org/10.1007/s11661-002-0314-z.

[Labus and et.al.(2014)] Labus and et.al. Influence of nitrogen and air atmosphere during thermal treatment on micro and nano sized powders and sintered tio2 specimens. *Science of Sintering*, 46(3):365–375, 2014. URL http://dx.doi.org/10.2298/SOS1403365L.

[Trunov and et.al.(2006)] Trunov and et.al. Oxidation and melting of aluminum nanopowders. *The Journal of Physical Chemistry B*, 110(26):13094–13099, 2006. URL https://doi.org/10.1021/jp0614188.

[Aharinejad and Lametschwandtner(1992)] SH Aharinejad and A Lametschwandtner. Fundamentals of scanning electron microscopy. In *Microvascular corrosion casting in scanning electron microscopy*, pages 44–51. Springer, 1992. ISBN 978-3-7091-9230-6. URL https://doi.org/10.1007/978-3-7091-9230-6_3.

[Hirschhorn and Roll(1970)] Joel S Hirschhorn and Kempton H Roll. *Advanced Experimental Techniques in Powder Metallurgy, ISBN= 978-1-4615-8981-5*. Springer, 1970.

[Zhou(2006)] et.al Zhou. Fundamentals of scanning electron microscopy (sem). In *Scanning microscopy for nanotechnology*, pages 1–40. Springer, 2006. ISBN 978-0-387-39620-0. URL https://doi.org/10.1007/978-0-387-39620-0_1.

[Ebnesajjad(2011)] Sina Ebnesajjad. 4 - surface and material characterization techniques. In Sina Ebnesajjad, editor, *Handbook of Adhesives and Surface Preparation*, Plastics Design Library, pages 31–48. William Andrew Publishing, Oxford, 2011. ISBN 978-1-4377-4461-3. URL https://doi.org/10.1016/B978-1-4377-4461-3.10004-5.

[He and Preckwinkel(2000)] B. He and et.al Preckwinkel. FUNDAMENTALS OF TWO-DIMENSIONAL X-RAY DIFFRACTION (XRD 2). *undefined*, 2000.

[Abd Mutalib and et.al.(2017)] M Abd Mutalib and et.al. Scanning electron microscopy (sem) and energy-dispersive x-ray (edx) spectroscopy. In *Membrane characterization*, pages 161–179. Elsevier, 2017. URL https://doi.org/10.1016/B978-0-444-63776-5.00009-7.

[Fricioni and Essig(1986)] R.B. Fricioni and Loren Essig. Inert Gas Fusion. In *Materials Characterization*. ASM International, 01 1986. ISBN 978-1-62708-178-8. doi: 10.31399/asm.hb.v10.a0001747. URL https://doi.org/10.31399/asm.hb.v10.a0001747.

[De Blasio(2019)] Cataldo De Blasio. *Fundamentals of biofuels engineering and technology*. Springer, 2019. ISBN 978-3-030-11599-9. URL https://doi.org/10.1007/978-3-030-11599-9.

[Wang et al.(2018)Wang, Rawal, Quadir, and Aguey-Zinsou] Lei Wang, Aditya Rawal, Md Zakaria Quadir, and Kondo-Francois Aguey-Zinsou. Formation of aluminium hydride (alh3) via the decomposition of organoaluminium and hydrogen storage properties. *International Journal of Hydrogen Energy*, 43(34):16749–16757, 2018. ISSN 0360-3199. URL https://doi.org/10.1016/j.ijhydene.2017.12.052.

LaTeX

DEPARTMENT OF SOME SUBJECT OR TECHNOLOGY
CHALMERS UNIVERSITY OF TECHNOLOGY
Gothenburg, Sweden
www.chalmers.se

CHALMERS
UNIVERSITY OF TECHNOLOGY